the interaction of the bare density oscillator $\Omega_0 \simeq 0.4\omega_p$ with the spectrum $q^2 D_L''(q, \omega)$ results in a three-peak structure of $S(q, \omega)$. One peak is situated at $\omega = 0$, one at $\omega \simeq 0.4\omega_p$ and the third at $\omega \simeq 0.9\omega_p$. This latter, small peak is the remainder of the peak at ω_0 in N_L'', which has been pushed to larger frequencies due to the coupling with bare oscillators at $\omega = 0$ and at $\omega = \Omega_0(q)$.

In Eq. (7) we have taken into account only those decay processes which are relevant for an understanding of the structure of φ_T'' and φ_ρ''. In reality, $N''(q, \omega)$ should have a small second peak situated at $\omega \simeq \omega_p$ which results from a decay into density fluctuations and longitudinal current excitations with small k. Besides producing a tiny bump at frequency larger than ω_p, the effect of this second maximum in $N''(\omega)$ will be a shift to lower frequencies and a decrease of the high-frequency peaks of φ_ρ'' and φ_T'' due to level repulsion. This is demonstrated by adding to Eq. (7) a similar term with resonance frequency ω_p, $\tau_{L2}^{-4} = 0.04\omega_p^4$, $\gamma_{L2} = \gamma_{T2} = 0.15\omega_p$, and $\tau_{T2}^{-4} = 0.02\omega_p^4$. The resulting spectra are also shown in Figs. 2 and 3. It is worth noting that $(\tau_L^{-4} + \tau_{L2}^{-4}) = 0.18\omega_p^4$ and $(\tau_T^{-4} + \tau_{T2}^{-4}) = 0.13\omega_p^4$ are consistent with the corresponding values calculated from the exact expressions for $\int d\omega N_{L,T}''(q, \omega)/\pi$ at $q = 3.094a^{-1}$ by using the Kirkwood superposition approximation for the static three-particle correlation function which enters: $(\tau_L^{\mathrm{KSA}})^{-4} = 0.217\omega_p^4$ and $(\tau_T^{\mathrm{KSA}})^{-4} = 0.143\omega_p^4$.[8]

Finally, we note that a two-peak structure in the shear-mode spectrum of liquid argon or liquid rubidium was not found. The reason for this is the different dispersion of longitudinal excitations for small q in liquids with short-range forces: The dispersion curve has a maximum at $q \simeq q_0/2$, $\omega = \Omega_E$ (Einstein frequency), and then vanishes linearly with q (see, e.g., Fig. 6 of Ref. 7). The maximum density of states is responsible for a large and broad contribution to $N''(\omega)$ around $\omega \simeq \Omega_E$. A too large and broad relaxation spectrum, however, will only lead to a shift and broadening of the bare oscillator Ω_T. It cannot produce a double-peak spectrum as observed in the OCP.

[(a)] On leave of absence from the Institute of Physics, Tsukuba University, Ibaraki, Japan.

[1] J.-P. Hansen, I. R. McDonald, and E. L. Pollock, Phys. Rev. A 11, 1025 (1975).
[2] W. Götze and M. Lücke, Phys. Rev. A 11, 2173 (1975).
[3] J. Bosse, W. Götze, and M. Lücke, Phys. Rev. A 17, 434 (1978).
[4] P. C. Martin, in *Problème à N Corps*, edited by C. de Witt and R. Balian (Gordon and Breach, New York, 1968).
[5] The relation to the transverse-current spectrum $C_t(q,\omega)$ used in Ref. 1 is given by $\omega_p \varphi_T''(q,\omega) = 3\pi \times \Gamma(aq)^{-2} C_t(q,\omega)/\omega_p$.
[6] J.-P. Hansen, Phys. Rev. A 8, 3096 (1973).
[7] J. Bosse, W. Götze, and M. Lücke, Phys. Rev. A 17, 447 (1978).
[8] J. Bosse and K. Kubo, to be published.

Observation of Extended Boundary Layers in the Permeative Flow of a Smectic-*A* Liquid Crystal around an Obstacle

Noel A. Clark
Department of Physics and Astrophysics, University of Colorado, Boulder, Colorado 80309
(Received 10 April 1978)

Experimental evidence is presented which supports the prediction of de Gennes of anomalous extended boundary layers accompanying the permeative steady-state flow of a single-domain smectic-A around an obstacle.

Although the essential feature of the smectic-A structure, namely the organization of molecules into fluid layers, has been known since the early work of Friedel,[1] it is only recently that the unusual macroscopic properties that derive from this structural fact have begun to be appreciated.[2,3] Of all of the predictions of new elastic-hydrodynamic effects perhaps the most remarkable arise from the anisotropic behavior of a smectic-A under conditions of steady flow. Steady-state flow with velocity components v_x, v_y parallel to the layer planes is governed by the Navier-Stokes equations; however, flow normal to the layers, v_z, is permeative: The molecules move as though through a porous plug which they themselves form.[4]

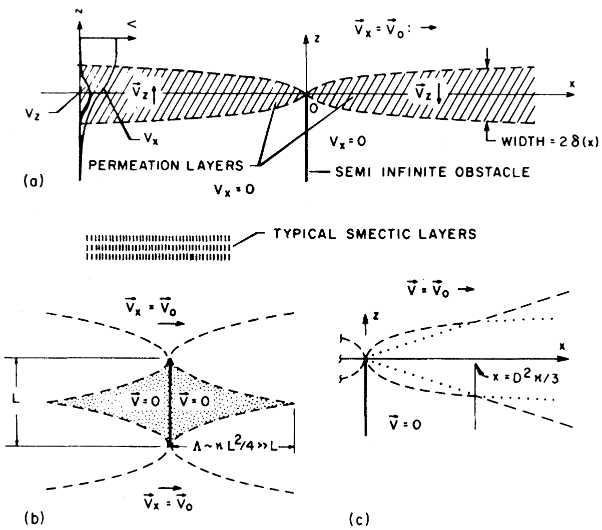

FIG. 1. Theoretical results for the flow of a smectic-A past a fixed obstacle. (a) Obstacle infinite in the $\pm y$ and z directions showing the permeation layers extending parallel to the smectic layers from the line where the obstacle ends (Ref. 5). (b) Obstacle infinite in the $\pm y$ direction and of width L along z. The static regions where $\vec{v}=0$ (dotted) continue to $x=-\Lambda$ $(+\Lambda)$ downstream (upstream) forming an extended boundary layer (Ref. 5). (c) The permeation layers for a sample of finite thickness D in the y direction. $\delta(x)$ is parabolic for $x<D^2\eta/3$ and linear for $x>D^2\eta/3$.

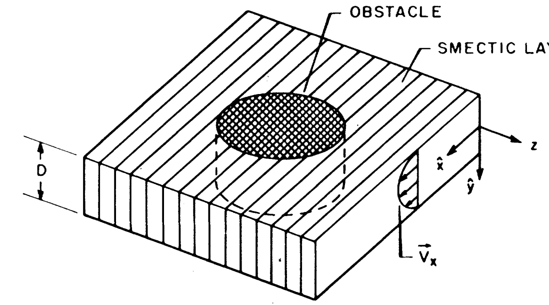

FIG. 2. Parallel sample geometry for observation of smectic flow. The "obstacles" are fixed bubbles which span the sample from glass to glass.

The application of the general hydrodynamic theory of smectics-A to specific flow problems and the realization of the novel effects which they describe was first made by de Gennes[5] and the Orsay group.[6] To illustrate a key prediction, I consider the steady flow at velocity $\vec{v}_x=\vec{v}_0$ of smectic-A past a planar obstacle oriented normal to the layers and of infinite extent in the y and z directions. In steady incompressible flow the velocity $\vec{v}(\vec{r})$ and pressure $p(\vec{r})$ are governed by the equations[5]

$$\begin{aligned}&\partial p/\partial z=-(1/\lambda_p)v_z\,,\quad \nabla\cdot\vec{v}=0,\\&\partial p/\partial x=\nu_3\partial^2 v_x/\partial z^2+\nu_2\partial^2 v_x/\partial y^2,\\&\partial p/\partial y=\nu_3\partial^2 v_y/\partial z^2+\nu_2\partial^2 v_y/\partial x^2,\end{aligned}\tag{1}$$

which show explicitly the abovementioned anisotropy. Here ν_2 and ν_3 are viscosities and λ_p is the permeation coefficient.[4] For the geometry of Fig. 1(a) one has $\partial/\partial_y, v_y=0$ and solutions for $v_x(x,z)$ and $v_y(x,z)$ which are indicated schematically in Fig. 1(a). The flow velocity $v_x(x,z)\cong 0$ for $z<-\delta(x)$ where $2\delta(x)$ is the local width of permeation layers (shaded areas) and $\delta(x)=(4|x|/\kappa)^{1/2}$. Here $\kappa^{-1}=(\nu_3\lambda_p)^{1/2}$ is a distance characteristic of the sample and should be on the order of a molecular length ($\kappa^{-1}\approx a\approx 20$ Å). There is permeative flow only in this layer with $-\partial p/\partial z$, $v_z>0$ for $z<\delta(x), x<0$ and $-\partial p/\partial z, v_z<0$ for $z<\delta(x), x>0$. If $\kappa^{-1}\approx 20$ Å, then the permeation layers will be extremely thin ($\delta\approx 5$ μm for $x=1$ mm and $\kappa^{-1}=20$ Å).

For an obstacle of finite extent, of width L along y as in Fig. 1(b), the permeative layers from the opposite ends will overlap only for x such that $2\delta\geq L$ or $x>\Lambda\cong\kappa L^2/4$.[5] Thus an obstacle of width L will block flow in an extended boundary layer reaching $x=-\Lambda$ upstream and $x=+\Lambda$ downstream [the dotted region in Fig. 1(b)]. For $L\approx 30$ μm and $\kappa^{-1}\approx 100$ Å one has $\Lambda\approx 2$ cm $\gg L$.

In this Letter I report the first evidence for this effect and support for the assumptions required to obtain Eqs. (1).[5]

The essential condition for the observation of permeative flow, namely the firm anchoring of the smectic layers, has been difficult to achieve in practice. At pressure gradients necessary to produce observable permeation, the layer structure pulls loose, is freed by nucleating dislocations, and is carried along in the flow. The geometry of the process of Fig. 1 is advantageous in this respect in that $\partial p/\partial z$ is nonzero only over very small spatial regions and that observable quantities, for example, Λ, are determined by a balance of viscous and permeative stresses.

The experimental geometry for the observation of permeative smectic flow is shown in Fig. 2. Single-domain samples of smectic cyanobenzylidene-octyloxyaniline (CBOOA) were prepared between glass slides obliquely evaporated with SiO and spaced by a distance D in the parallel geometry ($\hat{z}\parallel$ glass). Single domains were obtained by slowly cooling from the nematic and were highly ordered, allowing complete extinction of normally incident transmitted light polarized along the x or z directions. Experiments were carried out at $T = 78°\text{C}$. Firm layer anchoring was obtained by making the samples sufficiently thin, typically with $D \cong 1\ \mu\text{m}$.

Evidence for firm layer anchoring in this geometry is indicated in Fig. 3(a), which shows a typical sample in polarized transmitted light with the analyzer uncrossed. In this sequence of pictures, the area of entrapped bubbles which span the sample from glass to glass is increased by substantially decreasing D. The area expansion occurs by flow out along smectic layers which intersect the bubbles, leaving layers which do not intersect the bubbles fixed, and producing elongated bubbles. Bubbles with length to width ratios of 100:1 have been produced in this way.

Permeative smectic flow is observed in this geometry by introducing a fixed obstacle between the glass plates. In my experiments, bubbles which had become fixed to the glass by surface tension served as the obstacles. Unidirectional flow along the $-(+)x$ direction was produced by reducing D at large (negative) x.

The experimental situation is somewhat more complicated than that previously analyzed[5] and presented above, in that the sample is finite in the y direction so that flow requires $\partial v_x/\partial y, v_y$ to be nonzero and v_x is accompanied by a pressure gradient $-\partial p/\partial x$. Under the approximations of Eq. (1) this added complexity can be readily dealt with and leads to similar but quantitatively different behavior. For a sample of thickness D in the y direction the permeation layer width is now given by $2\delta(x)$ as indicated in Fig. 1(c):

$$\delta(x) = (4|x|/\kappa)^{1/2}, \quad |x| < D^2\kappa/3, \tag{2a}$$

$$\delta(x) = (\sqrt{12}/\kappa D)|x|, \quad |x| > D^2\kappa/3, \tag{2b}$$

where I have taken $\nu_2 = \nu_3$ for convenience.

For an obstacle of width $L \gg D$ we have $L \gg \delta \approx D$ at $x = D^2\kappa/3$ so that Λ is determined from Eq. (2b):

$$\Lambda = \kappa D L/4\sqrt{3}, \quad L \gg D. \tag{3}$$

The pressure gradient, $\partial p/\partial z$, across the permeation layer may be integrated to give the constant pressure p_s in the static ($\vec{v} = 0$) regions bounded by the permeation layers [dotted regions in Fig. 1(b)]. Taking $p(x,z) = 0$ in the y,z plane, the result is

$$p_s = (\pm)\frac{\sqrt{3}\kappa\nu_2 L}{D}, \quad x \ (\lessgtr)\ 0, \tag{4}$$

i.e., $p_s = p(x,z)$ at $x = +\Lambda$ $(-\Lambda)$ in the downstream (upstream) static region. Here $\langle v_x\rangle$ is the average flow velocity far from the obstacle $[\langle v_x\rangle = -(D^2/12\nu_2)\partial p/\partial x]$.

This pressure difference across the permeation layers drives the mechanism employed here to detect the flow. Referring to Fig. 1(b) in the upstream static region we have $p_s > 0$, and a net outward force per unit area exerted in the z direction tending to dilate these static layers. For $p_s > 2\pi(KB/L)^{1/2}$ this dilative stress will produce the smectic-A undulation instability, a dilation-induced periodic buckling of the layers,[7,8] in the upstream static region. Here K is the splay elastic constant and B the larger compression elastic constant. The appearance of the instability then provides a clear identification of the static region and the location of the permeation layers. Using measured values[8] of K and B and an estimate of $\nu_3 = 1$ poise in Eq. (4) the $\langle v_x\rangle$ required to generate the instability is $\langle v_x\rangle \approx 10^{-4}$ cm/sec. On the downstream side the situation is reversed, with $-(\partial p/\partial z)$ directed into the static region, producing dilation in the flowing regions just outside the permeation layers.

Our experimental observations of the undulation instability produced by flow past a 30-μm-diam fixed bubble are shown in Figs. 3(b) and 3(c). Here the sample is between crossed polarizers with the incident polarization in the z direction. Because of the excellent extinction, the small layer tilt associated with the undulation instability is readily visible. Figure 3(b) shows the pattern observed for flow in the $+x$ direction (upstream to the left) and Fig. 3(c) for the flow reversed (upstream to the right). The undulated (bright) regions observed are precisely those to be expected on the basis of the above considerations. I observe similar extended undulated areas associated with the edges of any discontinuity or defect in the sample (e.g., dust particles, borders, etc.) in the presence of flow. They are clearly visible, for example, in Fig. 3(a), emanating from the bubble edges parallel to the layers (arrows). Measurements of the extent of the undulated regions allow a crude lower limit to be placed on Λ and thereby an upper limit on the permeation length κ^{-1}. For $L \approx 30\ \mu$m and $D \cong 1$-μm boundary layers are observed to extend out to ~ 1 mm from the obstacle. Using Eq. (3) this requires $\kappa^{-1} \lesssim 100$ Å. The threshold velocity necessary to obtain layer distortion is consistent with the above estimate for $\langle v_x\rangle$ and was found experimentally by observing the motion of small parti-

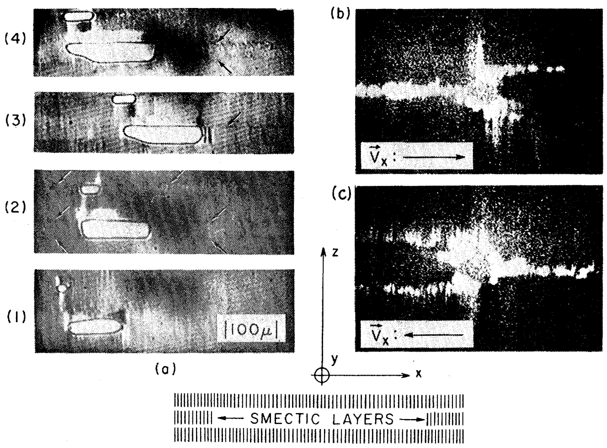

FIG. 3. Transmission micrographs of typical flow effects observed in thin single-domain CBOOA smectic-A samples in the parallel geometry, recorded on video tape (narrowly spaced horizontal lines are the TV raster): (a) Bubble distortion produced by decreasing D by about a factor of 2 going from (1) to (4). Significant flow occurs in the x direction only. Permeation layers extending along the smectic layers from where the bubbles are tangent to the layers are evident in (2), (3) and (4) (arrows). (b), (c) Undulated regions for a unidirectional flow $\vec{n}_x$, of relatively large magnitude in the + (−) x direction as indicated around a 30-μm wide fixed bubble (dark area in center). The undulated regions are visible out to $x = \pm 1$ mm. In Fig. 3(b) [3(c)] upstream is to the left (right).

cles carried in the flow. Generated flows were uniform over obstacle free sample areas—a condition difficult to obtain in thick samples because of focal conic defects. In thin samples ($D \approx 1$ μm), static focal conics are either suppressed by the boundary conditions or too small to be observed microscopically. *For low-velocity flows with* $\langle v_x \rangle$ *just over the threshold value for the appearance of the instability, the first observable distortions are on thin lines running parallel to the layers starting precisely from points where the boundary of any defect is tangent to the layers,* in accord with the theory of Fig. 1. Figure 3(a), panel (2) shows this effect most clearly. At the higher flows necessary to obtain the contrast of Figs. 3(b) and 3(c), the regions of maximal tilt recede somewhat from the low-velocity permeation layers [Figs. 3(b) and 3(c)], developing into parabolic focal conics[9] at high $\langle v_x \rangle$. All observable distortions abruptly disappear once the flow is stopped.

These observations provide the first evidence that the flow and stress patterns obtained by de Gennes using a far-field approximate solution[5] of the general smectic-A hydrodynamic equations applied to permeative flow is correct. Several further experiments are being attempted. In particular, if the velocity and sample thickness can be accurately controlled, then measurements of Λ vs D and L would allow a quantitative determination of κ. The temperature dependence of κ near the nematic–smectic-A phase transition would be especially interesting.

We gratefully acknowledge the help of C. Rosenblatt and R. Pindak in the preparation of the glass slides. This work was supported in part by National Science Foundation Grants No. 76-22452 and No. MRL-DMR 76-01111 to the Division of Applied Sciences, Harvard University.

[1]G. Friedel, Ann. Phys. (Paris) 18, 273 (1922).

[2]P. G. de Gennes, J. Phys. (Paris), Colloq. 30, C4-65 (1969).

[3]P. C. Martin, O. Parodi, and P. S. Pershan, Phys. Rev. A 6, 2401 (1972).

[4]W. Helfrich, Phys. Rev. Lett. 23, 272 (1969).

[5]P. G. de Gennes, Phys. Fluids 17, 1645 (1974).

[6]Orsay Liquid Crystal Group, J. Phys. (Paris), Colloq. 36, C1-305 (1975).

[7]N. A. Clark and R. B. Meyer, Appl. Phys. Lett. 22, 493 (1973); R. Ribotta and G. Durand, J. Phys. (Paris) 38, 179 (1977).

[8]N. A. Clark, Phys. Rev. A 14, 1551 (1976).

[9]C. S. Rosenblatt, R. S. Pindak, N. A. Clark, and R. B. Meyer, J. Phys. (Paris) 38, 1105 (1977).

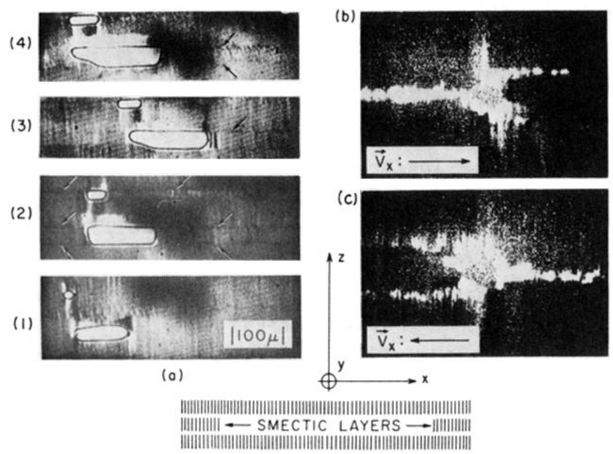

FIG. 3. Transmission micrographs of typical flow effects observed in thin single-domain CBOOA smectic-A samples in the parallel geometry, recorded on video tape (narrowly spaced horizontal lines are the TV raster): (a) Bubble distortion produced by decreasing D by about a factor of 2 going from (1) to (4). Significant flow occurs in the x direction only. Permeation layers extending along the smectic layers from where the bubbles are tangent to the layers are evident in (2), (3) and (4) (arrows). (b), (c) Undulated regions for a unidirectional flow $\vec{n}_x$, of relatively large magnitude in the + (−) x direction as indicated around a 30-μm wide fixed bubble (dark area in center). The undulated regions are visible out to $x = \pm 1$ mm. In Fig. 3(b) [3(c)] upstream is to the left (right).